by M. Copel

Mediumenergy ion scattering for analysis of microelectronic materials

This paper reviews the application of mediumenergy ion scattering (MEIS) to the study of materials problems relevant to microelectronics fabrication and reliability. Associated physical mechanisms and techniques are described. Three examples of MEIS studies are discussed in detail: Studies of the nucleation of silicon nitride on silicon dioxide, the interfacial segregation of Cu from Al(Cu), and the structure of hydrogen-terminated silicon surfaces created by various wet etching techniques.

Introduction

Progress in microelectronics is usually measured by how successful we are in shrinking the lateral size of devices, but we often overlook the remarkable decrease in the vertical dimensions of many device components. For example, while early CMOS devices used oxide layers that were 1000 Å thick, today's technology relies on films that are less than 100 Å thick. Current efforts are directed at films that are only dozens of atomic layers thick [1]. The reduction in vertical dimensions is the direct result of CMOS scaling laws.

For those concerned with the materials problems associated with device fabrication, the trend toward considerably thinner films has several implications. First, we must be increasingly concerned with their surface and interfacial properties. Second, as their thicknesses decrease, traditional analytic techniques will not be effective for many of the problems we encounter. The latter difficulty presents opportunities for surface science techniques to supplant bulk materials analysis techniques. But for a technique to be useful, it must be quantitative, versatile, and easy to interpret.

This paper describes the application of MEIS to microelectronics materials problems. First, we review the development of the technique and its underlying physical mechanisms. We then describe selected studies that illustrate how the combination of quantitative analysis with nanometer depth resolution and *in situ* processing is an effective way to investigate critical issues in microelectronics materials science.

Techniques

MEIS is based on the principles of Rutherford backscattering (RBS) of energetic ions. Since RBS analysis of solids is a well-established field, described in numerous books, we give only a brief explanation here [2, 3].

©Copyright 2000 by International Business Machines Corporation. Copying in printed form for private use is permitted without payment of royalty provided that (1) each reproduction is done without alteration and (2) the Journal reference and IBM copyright notice are included on the first page. The title and abstract, but no other portions, of this paper may be copied or distributed royalty free without further permission by computer-based and other information-service systems. Permission to republish any other portion of this paper must be obtained from the Editor.

0018-8646/00/\$5.00 © 2000 IBM

Essentially, an incident ion that encounters a solid at energies higher than 10–20 keV does not interact very strongly with the electron sea. Instead, the ion proceeds relatively unimpeded through the solid, unless it experiences a scattering event with one of the atomic cores. The core collisions are relatively rare events, so we are generally concerned with ions that penetrate a solid, undergo a single core collision, then re-emerge to be detected. The core collisions take place only when an ion passes within 0.01 Å of a nucleus, in which case the ion/core interaction is described by a screened Rutherford cross section, viz.

$$d\sigma/d\Omega = (z_{\text{ion}} z_{\text{target}} e^2 / 4E)^2 / \sin^4(\theta/2) \cdot V_{\text{screen}}, \tag{1}$$

where $z_{\rm ion}$ and $z_{\rm target}$ are the ion and target atomic numbers, E is the incident energy, θ is the scattering angle, and $V_{\rm screen}$ is an angle-independent, slowly varying screening term that is near unity. The re-emerging ion does not retain all of its initial kinetic energy. There are two important energy-loss mechanisms. In the first, the ion loses energy because of the scattering kinematics during core collisions. The kinematics are simply dictated by billiard-ball scattering; they follow the familiar equations that dictate two-body collisions:

$$E_{\text{ion}} = K(M_{\text{ion}}, M_{\text{target}}, \theta) E_{\text{inc}}, \tag{2}$$

where $K(M_{\rm ion}, M_{\rm target}, \theta)$ is an analytically known kinematic scattering factor. Using Equation (2) we are able to deduce the atomic mass of elements contained in the sample from the energy of the backscattered ions. This proves quite useful for analysis of samples of unknown composition.

A second energy-loss mechanism involves ion/electron interactions. As the ions penetrate the solid, they lose energy quasi-continuously to the electron sea. The energy loss is directly related to the ion path length. Hence, the inelastic energy loss at a given depth is increased by placing the detector at a more glancing exit angle. In the range of 50-200 keV, the rate of energy loss for H⁺ or He⁺ (known as the stopping power) is between 10 and 40 eV per Å of sample thickness, depending on the sample composition and density, ion species, and energy. (The stopping power of ions in solids has been the subject of extensive studies by J. Ziegler and coworkers, and values calculated from the Biersack-Ziegler formulas work fairly accurately in our energy regime [4]. For example, MEIS results for silicon nitride, described later in this paper, can be closely fitted with a stopping power of 44 eV/Å; the Biersack-Ziegler estimate is 39 eV/Å.) After correcting for the path length, the stopping power may be increased to 30 to 160 eV/Å of sample thickness. Since the energy resolution of the combined MEIS accelerator and detector is 120 eV for 100-keV protons, subnanometer depth resolution can be achieved. Unfortunately, such an

impressive depth resolution can be achieved for only relatively thin films ($<100\,\text{ Å}$). For thicker films, the resolution is severely hampered by energy straggling, the stochastic broadening of the ion energy distribution with increasing depth. But much of the interesting physics of nucleation and interface formation takes place in the initial stages of growth, so the limited depth range is a relatively minor inconvenience.

For the special case of crystalline substrates, additional techniques can be used to explore the sample composition. When the ion beam is aligned within $\sim 0.2^{\circ}$ of the crystal axis, the ions can channel through the substrate. The first few layers of the crystal shadow the underlying material, leading to greatly enhanced surface sensitivity. Furthermore, this allows us to quantitatively measure the extent to which a film is epitaxial. An additional benefit of channeling is the substantial reduction in the background signal from the substrate. The backscattered ion yield from a typical Si crystal is reduced to 2% of the random yield. This is crucial for light-element analysis, since the kinematic scattering factor, K, decreases with target mass. Consequently, ions backscattering from lighter elements have lower kinetic energies. For example, the oxygen signal from a SiO, layer on a silicon substrate occurs below the leading edge of the silicon signal. Unless the crystal is aligned with a channeling geometry, the signal from the silicon will overwhelm the signal from the oxygen. But if the bulk silicon signal is reduced by channeling, MEIS can be used to detect oxygen with a sensitivity of about 0.1 monolayer (ML). The main disadvantage of channeling experiments is that proper alignment for channeling requires a precision three-axis goniometer.

There are several key distinctions between MEIS and similar techniques such as RBS or high-energy ion scattering (HEIS). MEIS systems generally use ion energies that are much lower than in conventional RBS. Although this limits the depth we can reasonably probe to ~200 Å, there are several compensating benefits. Perhaps the most fundamental advantage is instrumentation. RBS analysis depends on the use of depleted silicon detectors, which are generally limited to an energy resolution of ~15 keV. But medium-energy ions have kinetic energies less than 300 keV, and can be deflected by electrostatic elements. Consequently, it is possible to construct an electrostatic energy analyzer for MEIS with resolution determined by the analyzer field strength and the size of various slits. Such an analyzer was designed and fabricated by Smeenk et al. and is now commercially available from High Voltage Engineering Europa B. V. [5]. The analyzer elements are toroidal sectors, allowing the simultaneous measurement of a 20° range of scattering angles (Figure 1). The toroidal sectors were originally configured with 0.5-mm entrance and exit slits. Behind the exit slit resides

572

a channel plate array with a patterned collector designed for one-dimensional position-sensitive detection of ions. The position-sensitive collector enables determination of the angle at which backscattered ions are detected. The ion energy is set by the analyzer field strength. More recently, the one-dimensional detectors have been replaced with two-dimensional detectors, an innovation that was developed at IBM [6]. This major enhancement has allowed the concurrent collection of ions spanning several keV and a broad range of angles. The principle of operation is quite similar to those of other energydispersive detectors. Since the energy window is set by the exit slit of the toroidal analyzer, the exit slit can be removed and a range of energies can be probed. However, a two-dimensional detector now becomes imperative to sort out the ion energies and angles. Since the exit slit of the analyzer is an arc, a straightforward rectangular detector will hopelessly convolute scattering angle with energy. The solution we have pursued is to develop a "backgammon"-patterned detector with radially arranged sectors (Figure 2). The new design has resulted in a twofold improvement in energy resolution while simultaneously increasing the count rate fivefold. Few of the experimental results described in this paper would have been feasible without the new detector, which made it practical to detect light elements such as oxygen and nitrogen and was crucial to implementing recoil detection of hydrogen. The detector has been commercialized through High Voltage Engineering Europa B. V., and has been installed in numerous MEIS systems worldwide.

In addition to the instrumental capabilities described above, the MEIS system used in this work is equipped for in situ processing experiments. The detector and goniometer are housed in an ultrahigh-vacuum (UHV) system with a sample exchange facility. The sample holders are capable of withstanding sustained sample heating, with short intervals at temperatures as high as 1200°C. This makes it possible to thermally reduce the native oxide layer normally found on silicon samples and initiate experiments with bare silicon surfaces. The main analytical system is coupled to an evaporation system with multiple sources, a Leybold-Hereaus hemispherical electron spectrometer with a SPECS multichannel detector, and both ultraviolet and X-ray sources. A UHV reactor cell is also available for studies of chemical vapor deposition and oxidation/nitridation reactions. The availability of such a wide array of processing tools and diagnostics has made possible the studies described below.

Experiments

Silicon oxynitrides

The silicon dioxide layer used as a gate insulator for MOSFETs has an impressively low density of electrically

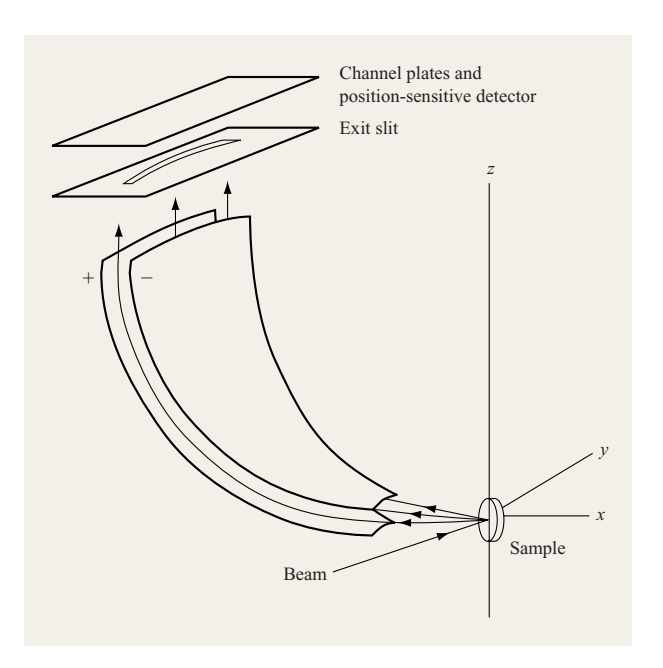


Figure 1

Schematic of apparatus for medium-energy ion scattering. Backscattered ions are energy-filtered by the toroidal electrostatic analyzer and are detected by the channel plate array. The charge cloud is collected on a position-sensing anode. From [5], with permission.

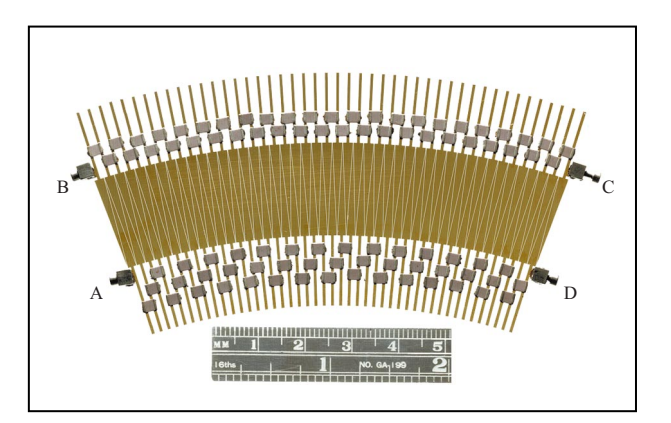


Figure 2

Photograph of two-dimensional position-sensitive collector. A charge cloud from the channel plates is collected on the wedges. The charge is then divided among the four outputs, A, B, C, and D. The ratios of the charge pulses are used to calculate the positions of the ions.

active defects, with mid-gap densities commonly in the range of $10^{10}/\text{cm}^2$. We must compare this to the detection threshold of typical surface science probes, where

sensitivities of 10¹³/cm² are considered acceptable. With this wide discrepancy, it would seem to be a formidable task to contribute anything useful to gate dielectric characterization with a surface structure probe. There are two ways to overcome this obstacle. One approach is to rely on the various scanning microscopies that can isolate and study defect regions. Alternatively, one can study materials that are potential replacements for silicon dioxide, such as oxynitrides. Oxynitrides offer an additional degree of freedom that is not present in pure oxide dielectrics: the ability to tailor the composition profile. But in order to take advantage of the extra flexibility, we must determine what the optimum profile is and how to achieve it. These are questions that do not require sensitivities comparable to those of electrical measurements, but do require a quantitative method of depth-profiling insulators with nanometer resolution. Increased concern with the reliability of extremely thin gate oxides has made the study of alternatives to SiO₃ a particularly urgent task [7].

A large body of work is devoted to the properties of oxynitrides and nitrides [8]; rather than reviewing this work, we simply point out a few features that are relevant to the present discussion. When dilute concentrations of nitrogen are included in SiO₂, there are beneficial effects, but there are also disadvantages. Among the benefits is an increased resistance to dopant indiffusion from the adjacent polysilicon layer, which can penetrate the gate oxide and enter the channel. In addition, films containing heavy concentrations of nitrogen should have an increased dielectric constant, which we hope will reduce the tunneling current for a given equivalent oxide thickness. But using nitrogen has several disadvantages. For undetermined reasons, when nitrogen is included in an oxide matrix, a small electrical charge is induced. The charge can be observed in electrical measurements as a flatband voltage shift. Not only is the flatband voltage shift undesirable, but if the nitrogen atoms are in charged states, they may act as carrier scatterers, reducing device mobility.

In the past, the nitrogen profiles of gate oxides have been largely determined by the vagaries of processing conditions. MEIS studies by Gustafsson and co-workers at Rutgers University have been instrumental in establishing a quantitative basis for the understanding of oxide nitridation [7, 9]. An example of the difficulties associated with tailoring oxynitrides is N₂O oxidation. N₂O reacts to leave nitrogen at the silicon/oxide interface, but can also etch nitrogen away from the bulk of the oxynitride, with the balance between nitrogen etching and deposition determined by reactor conditions [10]. This leaves only a very limited opportunity to tailor the profile, generating a small quantity of interfacial nitrogen under the most common reactor conditions. The resulting profile is, in

fact, particularly disadvantageous, since the nitrogen is quite close to the silicon/SiO₂ interface. If, instead, the nitrogen were placed as far from the Si/SiO₂ interface as possible, many of the benefits of nitrogen could be realized while minimizing the deleterious effects. By placing the nitrided layer near the doped polysilicon, we can hope to keep the dopants contained within the polysilicon layer and excluded from both the silicon channel and the dielectric. Also, if the nitrogen is placed as far from the channel as possible, the bulk of the dielectric can act as a screening layer, reducing any carrier scattering from the nitrogen-associated charge.

Now that we have proposed a gate dielectric structure, we are faced with the task of fabrication. This can be done either by reaction of gas species with the silicon substrate or by deposition of the film. At first glance, the former method would seem preferable. Reacted layers can be highly uniform, self-limiting and easily controlled, but because the reaction takes place at the Si/film interface, it is quite difficult to create a thin top layer near the dielectric/vacuum interface. This is because the top layer must first be fabricated, followed by each succeeding lower layer, until the Si/dielectric interface is finally created. Consequently, great care must be taken to avoid altering a nitrogen-rich top layer during subsequent processing. Several groups have shown that by careful control of oxidation conditions, it is possible to insert a pure SiO, spacer layer beneath a nitrided layer [8, 10, 11]. However, it may be difficult to extend this approach to achieving a true nitride-on-oxide structure. On the other hand, if a nitrided layer is deposited by chemical vapor deposition (CVD) above a thermal oxide as the final step in creating the gate dielectric, we can avoid numerous difficulties. Now we can be fairly confident that the nitrogen will remain confined to the top portion of the dielectric. Furthermore, the crucial silicon/dielectric interface can be formed at high temperature prior to nitride deposition. Also, the composition of the nitrogen-containing layer can be chosen at will. This gives an enormous degree of flexibility, permitting the use of pure silicon nitride rather than an oxynitride. Since the silicon nitride has a much higher dielectric constant than the oxide, there is the possibility of greatly increasing the thickness of the gate insulator without sacrificing capacitance. But to synthesize a successful nitride on oxide dielectric, the nitride must nucleate as a smooth, continuous pinhole-free film.

The nucleation of silicon nitride on silicon oxide is poorly understood, although it is critical to the fabrication of stacked dielectric structures. Previous investigators have grown silicon nitride layers on thermal silicon oxide, and have noted that the nitride layers thinner than a critical thickness are highly susceptible to oxidation [12]. This was taken as an indication that thin silicon nitride films are permeable, possibly containing pinholes. Furthermore, it

574

has been observed that there is a nucleation delay associated with nitride CVD on SiO₂, but not on bare silicon surfaces [13]. We have investigated CVD of silicon nitride on thermal oxide, and find that the nitride nucleates as islands which gradually merge to form a continuous film [14]. Nitride layers thinner than 20 Å are generally not continuous, rendering them unsuitable for use as gate dielectrics. The study included CVD films grown in two different ambients: a conventional CVD furnace using dichlorosilane and ammonia, and an *in situ* reactor using trisilylamine (TSA) and ammonia. Since similar results were obtained for the two ambients, it is likely that the morphology was due to the CVD temperatures and growth rates used rather than the specific precursor or reactor configuration.

The morphology of silicon nitride layers in the initial stages of growth can be deduced by comparing MEIS spectra for various silicon nitride films that were grown in situ. An easily prepared benchmark is a nitride layer grown by exposure of bare Si(001) to ammonia at elevated temperatures (for details, see Reference [15]). The nitridation reaction forms a smooth, continuous film of silicon nitride, and the MEIS spectrum shows a narrow nitrogen peak (Figure 3, labeled "RTN"). Another way of fabricating a benchmark sample is to evaporate a few atomic layers of silicon onto an oxidized silicon wafer at room temperature, and then gently heat the sample in ammonia. This also gives a relatively narrow nitrogen peak (Figure 3, labeled "Dep-RTN"). On the other hand, a sample prepared by CVD gives a nitrogen peak that is nearly twice as broad as the benchmark samples, even though it contains the same amount of nitrogen (Figure 3, labeled "CVD"). If the ions lose more energy penetrating the CVD nitride layer, they must penetrate deeper to get through the film. (This is caused by the stopping power, as mentioned in the Introduction.) Since the number of nitrogen atoms is the same in both cases, but they are distributed over a greater depth, the nitride layer must be rougher, perhaps even discontinuous.

The position of the oxygen peak is an additional indicator of film discontinuity in Figure 3. If the nitride layer is continuous, the oxide layer will be completely subsurface. Any ions that backscatter from the oxygen atoms must first penetrate the nitride layer, losing energy along the way. Thus, we would expect a shift in the position of the oxygen leading edge toward lower energy. In fact, that is exactly what is observed for the "Dep-RTN" benchmark, but there is no shift in the leading edge of the oxygen peak of the CVD nitride spectrum. This indicates that there is still surface oxide, and the nitride layer has not successfully covered up the oxide. It is worth noting that these observations would be extremely difficult without *in situ* analysis, since the inadvertent surface

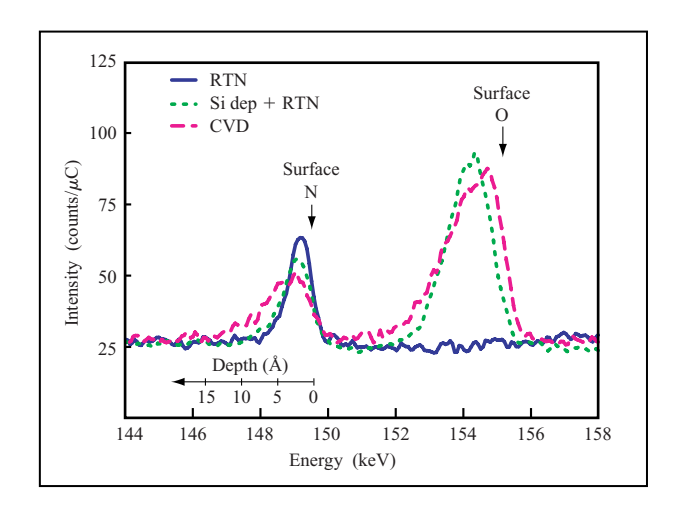


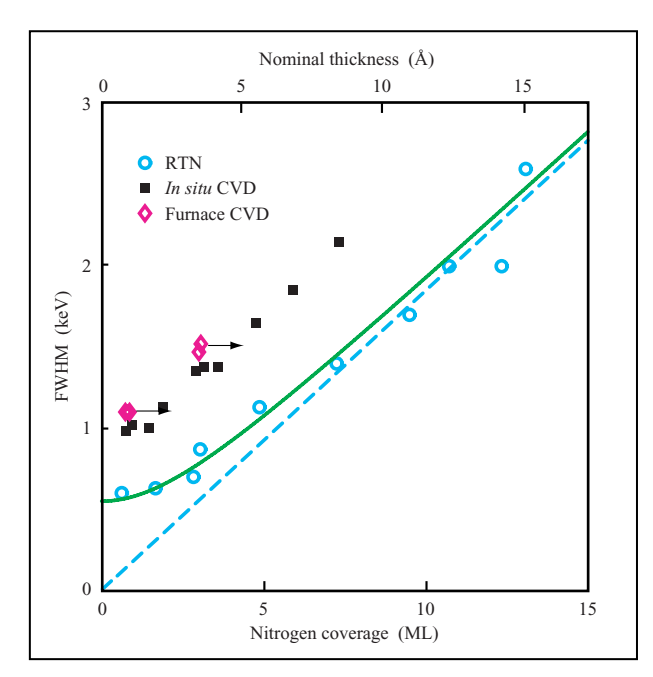
Figure 3

Ion backscattering spectra for silicon nitride films. The film grown by chemical vapor deposition (CVD) displays a broader nitrogen peak than do films grown by rapid thermal nitridation (RTN) or the nitridation of amorphous silicon (Si dep + RTN). The increase in nitrogen peak width indicates poorer film morphology. From [14], with permission.

oxidation caused by atmospheric exposure would greatly complicate the discussion.

Of course, a single spectrum can inform us about only one particular moment in the development of a film. However, we have examined a broad range of nitride thicknesses and found behavior similar to that shown in Figure 3. The results can be summarized by plotting the full width at half maximum (FWHM) of the nitrogen peak as a function of nitrogen content, after deconvoluting the detector resolution (Figure 4). For the entire range of nitrogen content shown, the nitride peak is significantly broader for the CVD films than for the RTN samples. We obtain similar results for in situ samples grown using TSA and for furnace-grown samples using conventional precursors, leading us to conclude that the growth mode is a characteristic of nitride nucleation on oxide at CVD temperatures and rates and is not specific to a particular ambient.

At higher coverages there is evidence of the nitride islands merging, but the interpretation of the data is complicated by the overlap of the nitrogen and oxygen backscattering peaks. We can still evaluate the films by comparing the data with simulated spectra. For example, in **Figure 5** we show a spectrum from a relatively thick nitride layer grown in a conventional low-pressure CVD furnace. The oxygen signal can be divided into two peaks: a narrow surface peak at 142.5 keV, and a broader peak at 139.7 keV due to the buried oxide layer. The region



Nitrogen peak width of silicon nitride films. The lower axis shows the nitrogen coverage, while the upper axis shows the nitride thickness, assuming a smooth continuous layer. The nitrogen peaks of films grown by chemical vapor deposition (CVD) are found to be systematically broader than films created by nitridation of silicon. The CVD data deviates strongly from the stopping power of silicon nitride (dashed curve), even when inelastic broadening is included (smooth curve). The arrows correct the *ex situ* furnace data for the effects of atmospheric exposure. From [14], with permission.

between the two peaks corresponds to the depth at which the film is predominantly nitride. Two simulated spectra are drawn. The dashed curve models the yield from a 15-Å-thick nitride layer sandwiched between a thin surface oxide and an underlying oxide. This model overestimates the depth of the valley between the two oxide peaks. If the nitride layer is assumed to contain 10% oxygen, the fit matches the data more closely (dotted curve). The oxygen could be the result of either post-growth oxidation or oxidized pinholes. In either case, roughly 10% of the film must be regarded as defective.

Our results show that the early stages of silicon nitride growth on oxidized substrates consist of island formation. Eventually, the islands merge to form a continuous film. It is likely that the initial island growth stage is associated with the nucleation period, when the islands may be quite difficult to detect by standard ellipsometric techniques. Alternative methods of growing silicon nitride, such as plasma CVD, may result in improved morphology for ultrathin films.

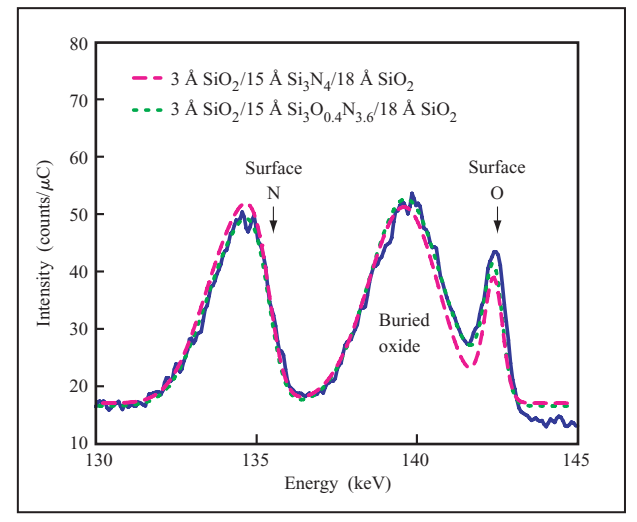
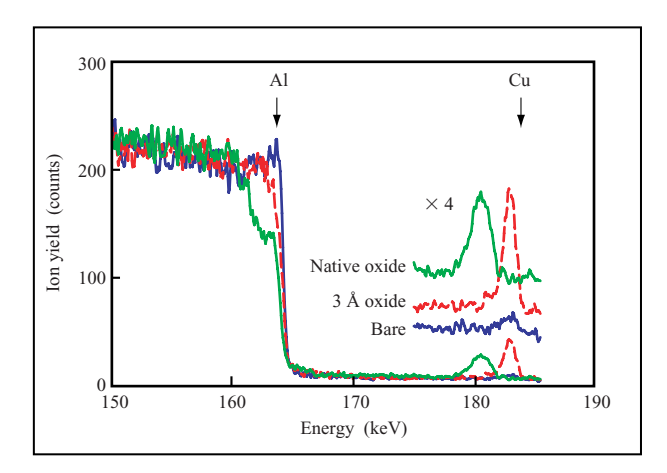


Figure 5

Ion backscattering spectrum for an *ex situ* chemical-vapor-deposited nitride layer on a thermally oxidized substrate. If the layer is modeled as stoichiometric Si_3N_4 (dashed curve), the depth of the valley between the surface oxide and the underlying oxide film is underestimated. A more realistic model incorporates some oxygen in the nitride (dotted curve), indicating either penetration of oxygen into the nitride or the presence of inhomogeneities such as oxidized pinholes. From [14], with permission.

• Cu segregation at Al(Cu)/oxide interfaces

Current-induced electromigration of on-chip wiring is a serious reliability concern in microelectronics. The addition of small amounts of Cu stabilizes Al lines against electromigration so effectively that Al(Cu) alloys have been widely employed as a wiring material [15]. Much of our understanding of electromigration phenomena is based on studies of Al and Al(Cu), so this remains an important system, despite the replacement of Al(Cu) with pure Cu in many applications. In the past, much of the effort has been devoted to grain-boundary segregation of impurities [16, 17], since the electromigration occurs predominantly at grain boundaries [18]. However, with decreasing linewidth, the metal/passivant interface becomes the dominant path for electromigration. Experimentally, there is an incubation period for electromigration in polycrystalline Al(Cu) lines, possibly corresponding to slow Cu electromigration, followed by catastrophic breakdown due to void formation [19]. Thus, electromigration in alloys may be strongly influenced by the composition of the metal/passivant interface. This section describes MEIS studies of the composition of the Al(Cu)/oxide interface [20]. Our results show conclusively that the interfacial composition is nearly two orders of



Al(Cu) samples annealed in ultrahigh vacuum. No Cu is found on a sample that is oxide-free, but interfacial Cu segregates upon annealing a sample having a thin oxide layer. When a thicker oxide is present, the Cu peak is shifted to lower energy, following the position of the Al(Cu)—oxide interface. From [19], with permission.

magnitude richer in Cu content after typical annealing conditions.

First, we consider the conditions under which Cu segregation is observed from a polycrystalline Al(0.18 at.% Cu) sample. When the sample is cleaned and annealed in UHV, only a very small quantity of Cu is observed on the surface (Figure 6, labeled "Bare"). Theoretical evaluations of the surface energies of metals indicate that Al has a substantially lower surface free energy than Cu, so Cu segregation to the bare surface is not expected [21]. However, if the same sample is lightly oxidized and again annealed, abundant quantities of surface Cu can be found. The Cu coverage increases from 0.01 ML to 0.18 ML in the presence of the surface oxide layer. [Here we define a ML based on the density of Al(111).] The oxide layer is only 3 Å thick, so it is highly unlikely that the Cu is an impurity in the oxide layer. When the oxide layer is much thicker, the Cu peak is displaced toward lower energy, following the expected position for the Al/oxide interface. Furthermore, the area of the Cu peak remains roughly the same, indicating that the segregational behavior does not change much with the oxide thickness. On the basis of chemical intuition, the appearance of interfacial Cu is rather surprising, since the energy of an Al-O bond vastly exceeds the energy of a Cu-O bond. It is difficult to imagine that it would be energetically favorable to break any Al-O bonds to accommodate the Cu, but the lattice mismatch between the aluminum oxide layer and Al may give rise to highly strained interfacial sites. If this is the

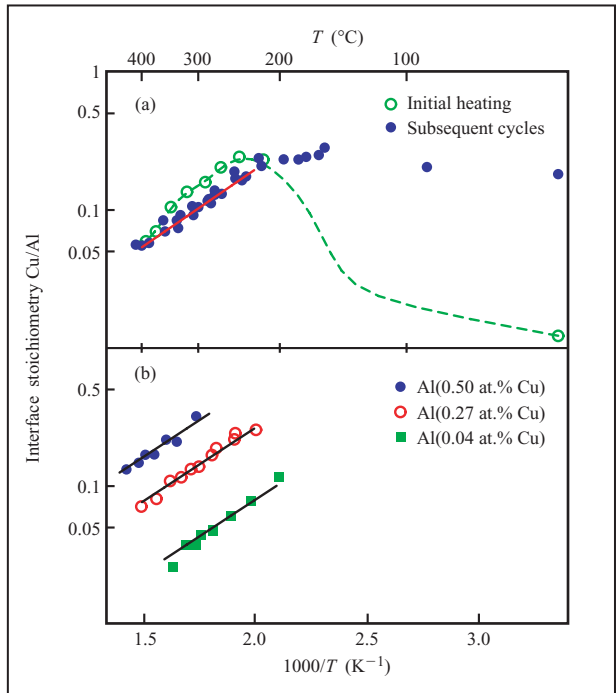


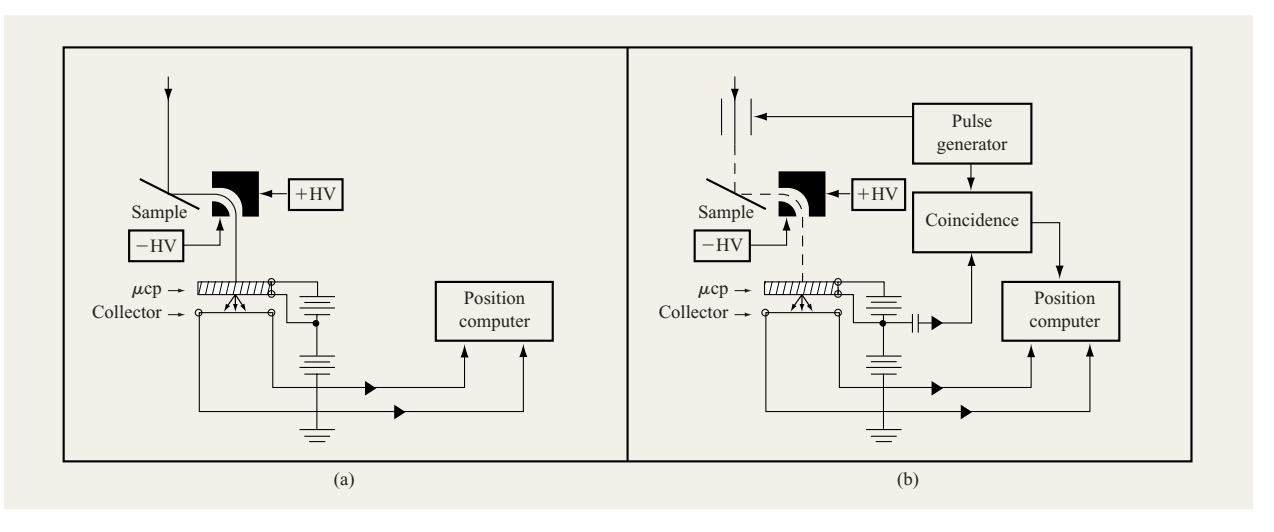
Figure 7

Interface composition of Al(Cu) samples at elevated temperatures: (a) After the initial annealing (circles), results are reproducible over many thermal cycles (solid dots). As the temperature increases above 200°C, the Cu dissolves back into the bulk. The solid line is modeled using a fixed enthalpy of segregation. The dashed curve is drawn to guide the eye. (b) Samples with a variety of bulk compositions exhibit similar temperature dependences of the Cu segregation, with the quantity of interfacial Cu being determined by the bulk composition. From [19], with permission.

case, the strain could be relieved by replacing some of the Al atoms with Cu, which have an 11% smaller radius.

Since segregation is dependent on both time and temperature, it is difficult to extract useful information by "postmortem" analysis at room temperature. We circumvented this difficulty by taking MEIS data with the sample at elevated temperatures. Since the accuracy of the measurement depended on precise integration of the ion beam dose, the sample was heated by an electrically isolated automobile battery. This provided a stable heating current for several hours of measurement, allowing the interfacial Cu concentrations to reach equilibrium.

The result of annealing a typical sample with an intact native aluminum oxide layer is shown in **Figure 7(a)**. The interfacial stoichiometry, $C_{\rm int}$, defined as the ratio of Cu/Al concentration at a hypothetical interfacial monolayer, is plotted for several cycles of heating and cooling. Prior to any heating, there is a negligible concentration of Cu at the interface. However, after heating to 250°C, $C_{\rm int}$



Experimental equipment for (a) routine medium-energy ion scattering and (b) enhancements for time-of-flight discrimination. Beam chopping and coincidence gating of the position computer are needed to distinguish recoiling hydrogen ions from elastically scattered lithium ions. Adapted from [28], with permission.

increases rapidly. $C_{\rm int}$ is observed to decrease with further heating, for entropic reasons. With further heating and cooling cycles, the Cu concentration follows the same pattern at high temperatures, but at temperatures below 200°C the Cu concentration is frozen on the time scale of our experiments.

The decrease in $C_{\rm int}$ at elevated temperatures can be analyzed using basic thermodynamic theories that describe interfacial segregation [22]. If we define $E_{\rm seg}$ as the enthalpy of segregation, $C_{\rm int}$ should follow an Arrhenius curve of the form

$$C_{\text{int}} = C_0 \exp\left(-E_{\text{seg}}/kT\right). \tag{3}$$

In the ideal case, C_0 is simply the bulk stoichiometry $(C_{\rm bulk})$. From **Figure 7(b)**, we can see that for various bulk compositions, the interfacial concentrations do indeed follow an Arrhenius curve, as described by Equation (3). Furthermore, the prefactor scales with the bulk composition. By fitting data from a wide range of bulk concentrations, we have determined an enthalpy of segregation of 0.21 ± 0.03 eV and a prefactor of $0.7 \times C_{\rm bulk}$. The solid lines plotted in Figures 7(a) and 7(b) are calculated using the best-fit value of $E_{\rm seg}$, and show that a single value works quite well over a wide range of Cu concentrations.

Throughout this discussion of Al(Cu) we have omitted discussion of Al₂Cu precipitates, which have commonly been observed in studies of Al(Cu) alloy films containing about 0.3 to 3 at.% Cu. If precipitation occurred, the precipitates would act as a sink for Cu, effectively removing dissolved Cu from the sample and from the

interface. This would cause a kink in Figure 7 at the onset of precipitate formation. The absence of precipitates is probably a result of the relatively low Cu concentrations used in this study, which are two to four times smaller than the concentrations commonly used to study precipitate formation [23].

From our results it can be safely concluded that the composition of an Al(Cu) alloy film at the interface with a surrounding oxide layer can be quite different than within the film. Indeed, unless such films are either quenched from high temperatures or entirely processed at room temperature, the interfaces will be Cu-rich. Although it remains unknown what role Cu plays in interfacial electromigration, a precise knowledge of the interfacial composition is a fundamental step in developing an understanding of that phenomenon. The equilibrium interface composition can be quite accurately predicted on the basis of the MEIS results.

• Hydrogen-terminated silicon surfaces

This section presents MEIS results on the structure of hydrogen-terminated silicon surfaces prepared by wet chemical procedures. Clean, damage-free silicon surfaces are an essential requirement for low-temperature epitaxial silicon growth. HF-last cleaning recipes have been highly effective for creating hydrogen-terminated surfaces that are air-stable and oxygen-free [24]. The chemical cleanliness and stability of the H/Si(001) surface is undoubtedly a remarkable achievement. However, surface roughness is an aspect of the H/Si(001) preparation that

578

remains less well controlled than chemical cleanliness. Generally, HF-based treatments attack silicon oxide but leave the unoxidized silicon intact, so the surface morphology is usually representative of the roughness of the Si–SiO₂ interface prior to etching [25, 26]. Consequently, surface polishing and repeated cycles of oxidation and etching are usually required in order to obtain a flat surface. However, it is possible to replace HF with a highly caustic NH₄F solution that etches anisotropically. Chabal and co-workers have shown that NH₄F-based etching can actually improve the surface smoothness on Si(111), resulting in domains of 100 Å [26]. Unfortunately, the anisotropy favors (111) planes and causes facet formation on Si(001).

Light elements are difficult to study with MEIS because the cross section for a core collision decreases with the square of the atomic number. For the case of hydrogen, there is no possibility of detection unless use is made of elastic recoil detection (ERD) [27]. The data shown previously in this paper were obtained by detecting backscattered ions (He⁺ incident, He⁺ detected). For ERD, we detect an ion that originates from the sample and recoils from the core collision (Li⁺ incident, H⁺ detected). Although ERD has been used by many groups with MeV ion beams, our work was the first using ion beams in the MEIS range [28]. Without any modification, a conventional MEIS apparatus can be used to detect recoiling protons; the difficulty is in distinguishing the recoil events from the much more common backscattering events. What is needed is a method for determining both the ion energy and species, allowing separation of the recoiling protons from the backscattered Li ions. Since the analyzer transmits only particles within a narrow range of energy, the Li ions and protons that are transmitted have quite different velocities. Thus, the flight time for the particles can be used to discriminate events.

For ERD, we use the same detector and electronics used in conventional MEIS, but with the addition of beam chopping and time-resolved detection (**Figure 8**). Since the flight time from sample to detector of a 50-keV H⁺ recoil and a backscattered 50-keV Li⁺ ion differs by 160 ns, a commercially available time-discrimination circuit is adequate for our purposes. The toroidal detector is still used for energy analysis, so the depth resolution is comparable to a normal MEIS measurement. MEIS-ERDA has been used as a technique to study the structure of H-terminated silicon surfaces [29], as well as the effect of surface H on silicide nucleation [30] and silicon homoepitaxy [31, 32].

The efficacy of solution-based NH₄F cleaning can be seen by comparing the MEIS spectrum for a wet-cleaned Si(111) sample with a sample that has been prepared by a brief flash to 1200°C in UHV [Figure 9(a)]. Both spectra

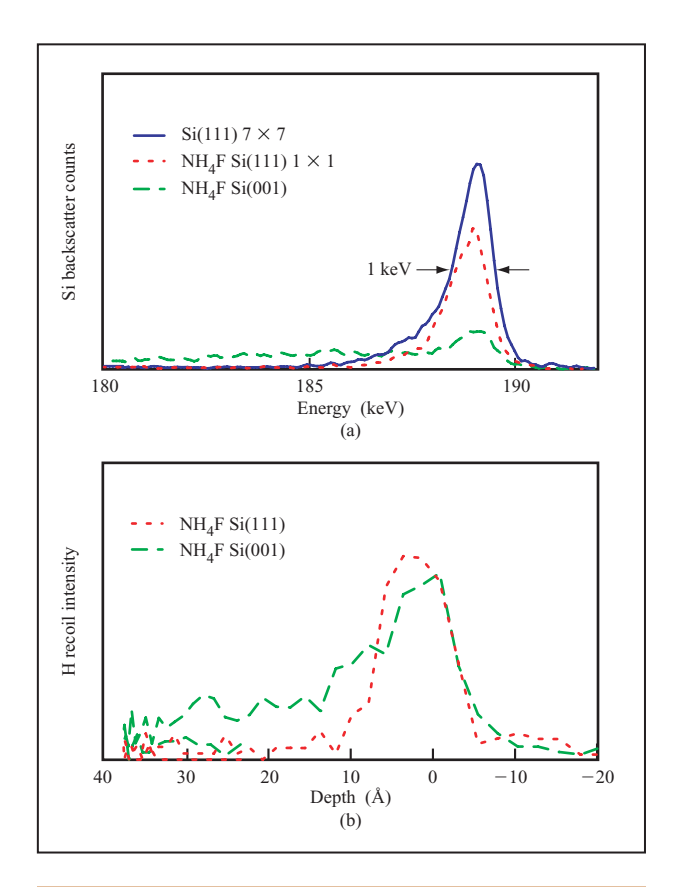
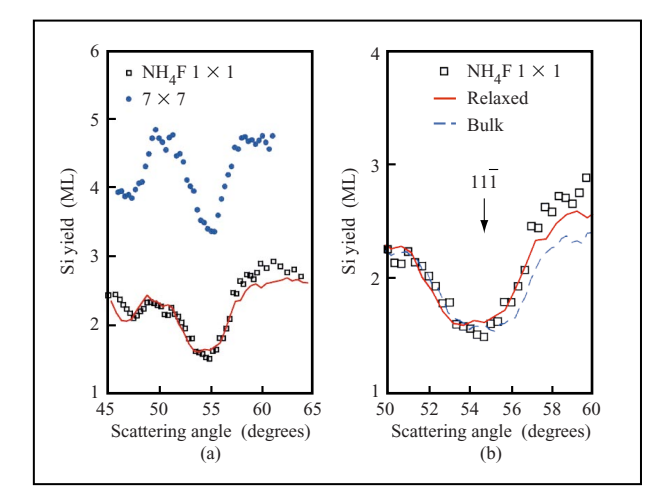


Figure 9

Silicon surfaces prepared either by oxide desorption in ultrahigh vacuum to create a bare surface, or by wet-etching with $\mathrm{NH_4F}$ to create a hydrogen-terminated surface: (a) The silicon surface peak is smaller for $\mathrm{Si}(111)$ prepared with $\mathrm{NH_4F}$ than the bare sample, because of the removal of the surface reconstruction. The surface peak from the $\mathrm{Si}(001)$ sample is broadened by faceting. (b) The H recoil profile shows a flat, monohydride termination for $\mathrm{Si}(111)$, but is also broadened for $\mathrm{NH_4F}$ -etched $\mathrm{Si}(001)$. From [29], with permission.

show a silicon surface peak (SP) of comparable width with no significant bulk background. The flash-cleaned sample, labeled 7×7 , displays a much larger SP than the NH₄F sample because of the displacement of atoms that participate in the 7×7 surface reconstruction. The reconstructed atoms do not occupy bulk lattice sites and are unable to shadow the underlying crystal. Consequently, the first 4–5 atomic layers are visible to the incident ion beam. On the other hand, the H-terminated surface is not reconstructed, so the first few atomic layers are sufficient to shadow the underlying crystal. We found an H coverage for the NH₄F-treated sample of 1.11 \pm 0.1 ML, as anticipated for a monohydride termination. The H depth profile is quite narrow, with all of the signal confined to the top 1 nm of the sample [Figure 9(b)].



Angular variation of the silicon surface peak for Si(111): (a) For the reconstructed surface, labeled 7×7 , surface atoms are unable to shadow underlying layers, leaving them visible to the ion beam. The hydrogen-terminated surface, prepared with NH₄F, is a bulk-like truncation, so fewer atomic layers are visible. (b) The position of the $(11\bar{1})$ blocking dip reveals any distortion of the surface interplanar spacing. In this case, the spacing is reduced by 0.07 Å. From [29], with permission.

If NH₄F is applied to Si(001) rather than Si(111), there is a striking change in both the Si surface peak and the H depth distribution. On Si(001), the Si surface peak is nearly eliminated, and a background signal appears extending more than 10 keV below the SP. The H signal shows a similar broadening. This is the result of microscopic surface roughening, which severely degrades the sample morphology. The faceting is so extensive that backscattered ions from valleys in the sample are unable to reach the detector without first passing through crests. The ions lose energy while passing through the crests, hence broadening both the Si SP and the H recoil peak.

To what degree does NH₄F treatment of Si(111) create an ideal surface? We can answer this question by quantitative analysis of the Si surface peak [Figure 10, part (a)]. The H-terminated surface shows a greatly decreased yield over a wide range of scattering angles. If we compare the yield with computer simulations of ion scattering from an ideally terminated Si(111) surface, the agreement is quite close. If any portions of the surface are reconstructed, or if any atomic debris remains from etching, the yield would exceed the expected result. Since the increase in yield would be linear with the portion of the surface that remained reconstructed, we safely estimate that less than 10% of the H-terminated surface deviates from the ideal truncation. The highly ordered surface is probably the

result of silicon etching by the NH₄F solution, which selectively removes the atomic debris.

The angular distribution of backscattered ions can also be used to determine the atomic structure of the surface. The Si surface peak shows a pattern of so-called blocking dips, which mark angles where backscattered ions are prevented from re-emerging into the vacuum. The blocking dips occur along the major crystallographic axes of the sample. If the surface structure is distorted from the bulk structure, the blocking dips undergo an angular shift. In the particular scattering geometry used in Figure 2, a decrease in the (111) interplanar spacing causes an angular shift of the blocking dip toward smaller scattering angles. By comparing the data with Monte Carlo simulations, we have determined that the results are best fitted by a 0.075 ± 0.03 -Å decrease in the outermost interplanar spacing, and a 0.03 ± 0.03 -Å decrease in the next interplanar spacing, in excellent agreement with firstprinciple theoretical models [33].

Concluding remarks

The continued downward scaling of semiconductor devices is gradually forcing both the use of new materials and new methods of materials analysis. This paper has described the application of MEIS to materials studies that are relevant to microelectronics. A unique strength of MEIS is its applicability to measurements spanning the crucial regime that links surface science with thin-film studies.

Acknowledgments

I wish to thank Ruud Tromp for many fruitful collaborations. I also would like to acknowledge the technical assistance of Mark Reuter and the help of many collaborators with whom I have had the honor of working.

References and notes

- The National Technology Roadmap for Semiconductors, Semiconductor Industry Association, Austin, TX, 1997.
- L. C. Feldman, J. W. Mayer, and S. T. Picraux, Materials Analysis by Ion Channeling, Academic Press, Inc., New York, 1982.
- 3. J. F. Van der Veen, "Ion Beam Crystallography of Surfaces and Interfaces," Surf. Sci. Rep. 5, 199 (1985).
- 4. J. F. Ziegler, J. P. Biersack, and U. Littmark, *The Stopping and Range of Ions in Solids*, Pergamon Press, New York, 1985; for a downloadable modeling program, see http://www.research.ibm.com/ionbeams/.
- R. G. Smeenk, R. M. Tromp, H. H. Kersten, A. J. H. Boerboem, and F. W. Saris, "Angle Resolved Detection of Charged Particles with a Novel Type Toroidal Electrostatic Analyser," Nucl. Instr. Meth. 195, 581 (1982); for a description of the commercially available analyzer, see R. M. Tromp, H. H. Kersten, E. Granneman, F. W. Saris, R. Koudijs, and W. J. Kilsdonk, "A UHV System for Channeling/Blocking Analysis of Solid Surfaces and Interfaces," Nucl. Instrum. Meth. B 4, 155 (1984).
- R. M. Tromp, M. Copel, M. C. Reuter, M. Horn-von Hoegen, J. Speidell, and R. Koudijs, "A New 2-D Particle

- Detector for a Toroidal Electrostatic Analyzer," Rev. Sci. Instrum. 62, 2679 (1991).
- J. H. Stathis and J. DiMaria, "Reliability Projection for Ultra-Thin Oxides at Low Voltage," *IEDM Tech. Digest*, p. 170 (1998).
- E. P. Gusev, H.-C. Lu, E. L. Garfunkel, T. Gustafsson, and M. L. Green, "Growth and Characterization of Ultrathin Nitrided Silicon Oxide Films," *IBM J. Res. Develop.* 43, 265–286 (1999).
- H. C. Lu, E. P. Gusev, T. Gustafsson, E. Garfunkel, M. L. Green, D. Brasen, and L. C. Feldman, "High Resolution Ion Scattering Study of Silicon Oxynitridation," *Appl. Phys. Lett.* 69, 2713 (1996).
- E. C. Carr, L. A. Ellis, and R. A. Buhrman, "N Depth Profiles in Thin SiO₂ Grown or Processed in N₂O: The Role of Atomic Oxygen," *Appl. Phys. Lett.* 66, 1492 (1995).
- N. S. Saks, D. I. Ma, and W. B. Fowler, "Nitrogen Depletion During Oxidation in N₂O," *Appl. Phys. Lett.* 67, 374 (1995).
- 12. K. K. Young, W. G. Oldham, and J. Rose, "Preparation and Characterization of 100Å Oxide/Nitride/Oxide Stacked Films," Silicon Nitride and Silicon Dioxide Thin Insulating Films, V. J. Kapoor and K. T. Hankin, Eds., The Electrochemical Society, Pennington, NJ, 1987, p. 471.
- F. Martin, F. Bertin, H. Sprey, and E. Granneman, "LPCVD Si₃N₄ Growth Retardation on Silicon Native Oxide Compared with *In Situ* HF Vapor-Deglazed Silicon Substrates," *Semicond. Sci. Technol.* 6, 1100 (1991).
- M. Copel, P. R. Varekamp, D. W. Kisker, F. R. McFeely, K. E. Litz, and M. M. Banaszak Holl, "Nucleation of Chemical Vapor Deposited Silicon Nitride on Silicon Dioxide," *Appl. Phys. Lett.* 74, 1830 (1999).
- F. M. d'Heurle and P. S. Ho, Thin Films—Interdiffusion and Reactions, J. M. Poate, K. N. Tu, and J. W. Mayer, Eds., Wiley, New York, 1978.
- 16. D. R. Frear, J. E. Sanchez, A. D. Romig, Jr., and J. W. Morris, Jr., "The Evolution of Microstructure in Al–2Pct Cu Thin Films: Precipitation, Dissolution, and Reprecipitation," *Meta. Trans. A* 21, 2449 (1990); J. R. Michael, A. D. Romig, Jr., and D. R. Frear, "Grain Boundary Chemistry in Al–Cu Metallizations as Determined by Analytical Electron Microscopy," *Mater. Res. Soc. Symp. Proc.* 229, 303 (1991).
- M. B. Small, D. A. Smith, and A. J. Garrat-Reed, "Segregation of Copper in Dilute Aluminum-Copper Alloys," Scripta Met. 30, 1531 (1994).
- C.-K. Hu, M. B. Small, K. P. Rodbell, C. Stanis,
 P. Blauner, and P. S. Ho, "Electromigration Failure Due to Interfacial Diffusion in Fine Al Alloy Lines," *Appl. Phys. Lett.* 62, 1023 (1993).
- C.-K. Hu, M. B. Small, and P. S. Ho, "Electromigration in Al(Cu) Two-Level Structures: Effect of Cu and Kinetics of Damage Formation," J. Appl. Phys. 74, 969 (1993).
- M. Copel, K. P. Rodbell, and R. M. Tromp, "Cu Segregation at the Al(Cu)/Al₂O₃ Interface," Appl. Phys. Lett. 68, 1625 (1996).
- A. R. Miedema, "Surface Energies of Solid Metals,"
 Z. Metallkde. 69, 287 (1978).
- 22. For a full discussion, see M. J. Sparnaay, "Thermodynamics (with an Emphasis on Surface Problems)," Surf. Sci. Rep. 4, 101 (1984), or A. Zangwill, Physics at Surfaces, Cambridge University Press, Cambridge, 1988, p. 85.
- E. G. Colgan and K. P. Rodbell, "Kinetics of Al Grain Growth, Al₂Cu Precipitation, and Dissolution in Blanket Thin Films and Fine Lines," *J. Appl. Phys.* 75, 3423 (1994) and references therein.
- B. S. Meyerson, "Low-Temperature Silicon Epitaxy by Ultrahigh Vacuum/Chemical Vapor Deposition," *Appl. Phys. Lett.* 48, 797 (1986);
 B. S. Meyerson, F. J. Himpsel,

- and K. J. Uram, "Bistable Conditions for Low-Temperature Silicon Epitaxy," *Appl. Phys. Lett.* **57**, 1034 (1990).
- G. S. Higashi, Y. J. Chabal, G. W. Trucks, and K. Righavachari, "Ideal Hydrogen Termination of the Si(111) Surface," *Appl. Phys. Lett.* 56, 656 (1990); G. S. Higashi, R. S. Becker, Y. J. Chabal, and A. J. Becker, "Comparison of Si(111) Surfaces Prepared Using Aqueous Solutions of NH₄F Versus HF," *Appl. Phys. Lett.* 58, 1656 (1991).
- G. J. Pietsch, U. Kohler, and M. Henzler, "Anisotropic Etching Versus Interaction of Atomic Steps: Scanning Tunneling Microscopy Observations on HF/NH₄F-Treated Si(111)," J. Appl. Phys. 73, 4797 (1993).
- For a review, see A. D. Marwick, in *Hydrogen in Semiconductors*, J. I. Pankove and N. M. Johnson, Eds., Academic Press, Berlin, 1991.
- M. Copel and R. M. Tromp, "Elastic Recoil Detection for Medium Energy Ion Scattering," Rev. Sci. Instrum. 64, 3147 (1993).
- M. Copel, R. J. Culbertson, and R. M. Tromp, "Relaxation and H Coverage of Ammonium Fluoride Treated Si(111)," *Appl. Phys. Lett.* 65, 2344 (1994).
- M. Copel and R. M. Tromp, "Nucleation of Co Silicide on H Passivated Si(111)," Appl. Phys. Lett. 65, 3102 (1994).
- 31. M. Copel and R. M. Tromp, "H Coverage Dependence of Si(001) Homoepitaxy," *Phys. Rev. Lett.* **72**, 1236 (1994).
- 32. M. Copel and R. M. Tromp, "Medium Energy Ion Scattering Investigation of Homoepitaxy on H Terminated Si(111)," *Surf. Sci. Lett.* **337**, L773 (1995).
- E. Kaxiras and J. D. Joannopoulos, "Hydrogenation of Semiconductor Surfaces: Si and Ge(111)," *Phys. Rev. B* 37, 8842 (1988).

Received April 14, 1999; accepted for publication August 2, 1999

Matthew Copel IBM Research Division, Thomas J. Watson Research Center, P.O. Box 218, Yorktown Heights, New York 10598 (mcopel@us.ibm.com). Dr. Copel is a Research Staff Member in the Physical Sciences Department at the Thomas J. Watson Research Center. He received a B.A. degree in physics from Harvard University in 1980, and a Ph.D. degree in physics from the University of Pennsylvania in 1986. Dr. Copel joined IBM in 1986 and initially studied semiconductor surface and epitaxial growth phenomena. In 1991, he received an IBM Outstanding Innovation Award for work on surfactants in epitaxial growth. His present research interests involve the properties of advanced dielectric materials.